

Optical and electrical characterization of an atmospheric pressure microplasma jet with a capillary electrode

Hye Sun Park,¹ Sun Ja Kim,² H. M. Joh,² T. H. Chung,^{1,2,a)} S. H. Bae,² and S. H. Leem³

¹*Department of Nano Engineering, Dong-A University, Busan 604-714, Republic of Korea*

²*Department of Physics, Dong-A University, Busan 604-714, Republic of Korea*

³*Department of Biological Science, Dong-A University, Busan 604-714, Republic of Korea*

(Received 25 November 2009; accepted 3 February 2010; published online 8 March 2010)

A microplasma jet with a capillary electrode working at atmospheric pressure is developed to create nonthermal plasma. This jet can be operated at an excitation frequency either in several tens of kilohertz ac range (or pulsed voltage with a repetition rate of kilohertz range) or in radio-frequency range. The working gas, helium or argon, and the additive gas, oxygen, are fed into the plasma jet. The discharge has been characterized by optical emission spectroscopy. The electrical property of the discharge has been studied by means of voltage and current probes. The dynamic nature of the plume is investigated by using intensified charged coupled device camera. The electron temperature is estimated from the modified Boltzmann plot method utilizing the Ar 4p→4s transitions. The plume temperature is determined by using the fitting the fine structure of the emission bands of OH molecules and by utilizing the line shape of the transition. They are compared with the results obtained by optical fiber thermometer. The characteristics of plasma jet are studied by employing different excitation mode and by adjusting the gas flow rates, the applied voltage, and the amount of additive O₂ flow. The characteristic differences between the Ar plasma jet and the He plasma jet are compared. The effects of the additive O₂ gas are investigated. The plasma bullet velocity is found to increase with the applied voltage but to decrease with the duty cycle. Also the preliminary results of microplasma effects on the human breast cancer cells are presented. © 2010 American Institute of Physics. [doi:10.1063/1.3330507]

I. INTRODUCTION

Nonthermal atmospheric pressure plasma jet devices have recently attracted significant attention due to their great potential for a variety of material processing and biomedical applications.¹⁻³ Especially, the biomedical applications of the plasma jet have become hot issues. Since plasma jet devices generate plasma plumes in open space surrounding air rather than in confined discharge gaps, they can be used for the direct treatment and there are no limitations on the sizes of the objects to be treated. One of the prerequisites to the biomedical applications is that the jet should be near the room temperature and carries a low current under moderate voltage. Another key challenge is to attain high plasma stability while maintaining efficient reaction chemistry.

The plasma generation in microplasma jets relies on various mechanisms: capacitively coupled discharge, corona discharge, and dielectric barrier discharge (DBD).⁴⁻⁶ The mechanism underlying nonthermal plasma jets, however, remains unsettled that it has been often taken as resulting from DBD or vaguely referred to as streamerlike. In particular, the single bare metal pin electrode can generate plasma jets of comparable lengths at a much reduced voltage, and it permits a very flexible and cost effective application of the plasma jet.⁷ Plasma jet operates at atmospheric pressure with a high-flow feed gas consisting of an inert carrier gas (typically helium) and a small amount of an additive gas such as O₂. It

is necessary to study the possibility to use argon to replace helium to produce a wide range of chemistry.⁸

When operating at higher frequencies, the plasma jet is formed by a continuous plasma flow. However, when operating at lower frequencies, it has been found that the plasma jet is constituted of discrete bulletlike plasma clouds moving at a velocity much higher than the gas velocity.⁸⁻¹¹ However, until now there have been few attempts to investigate the physical processes that can elucidate the way plumes are initiated and maintained in an atmospheric pressure environment. As will be confirmed later, the plasma bullet is actually an ionization wave front propagating at high speed. A special form of gas breakdown takes place in the case of a needle-shaped electrode that creates a nonuniform electric field. Then the ionization wave propagates in the form of a streamer. Recently a number of experimental studies have been carried out to understand the dynamic behavior of the plasma jet.⁹⁻¹² Images of the discharge were captured using an intensified charge-coupled device (ICCD) camera, and the propagation velocity of the plasma was also determined. Lu and Laroussi⁹ proposed a streamer discharge model to explain how the plume emitted by the plasma jet is produced. This model may apply to many of the cold plasma plumes used today. To have a plume travel at high speed under very low electric field, photoionization has to play an important role. In their photoionization-based model the head of a cathode-directed streamer is assumed to be a sphere, containing positive ions. As the streamer head moves forward, it leaves behind a quasineutral ionized channel with a very low

^{a)}Author to whom correspondence should be addressed. Electronic mail: thchung@dau.ac.kr.

conductivity; the head is not connected to the anode and only the streamer head is measurably luminous.

In this paper, a especially designed microplasma jet source driven by various types of power supply [several tens of kilohertz ac sinusoidal voltage, pulsed voltage with repetition rates of kilohertz range, and radio-frequency (RF) voltage] is reported. The use of Ar gas usually elevates the plume temperature of the plasma jets. One possible solution is to employ pulsed excitation to reduce plume temperature. This jet source has a capillary powered electrode through which additive O₂ gas can be injected. In order to have an in-depth understanding of the characteristics of the plasma plume, first the voltage-current (*V-I*) characteristics of the discharge are studied. The plume length, the plumes temperature, and optical spectra are measured as functions of the applied voltage, gas flow rate, and the excitation methods (pulsed wave, sinusoidal wave, and RF wave). The plume temperature is determined by using the fitting the fine structure of the emission bands of OH molecules and by utilizing the line shape of the transition. They are compared with the results obtained by optical fiber thermometer. Since the role of O atom is important in the interaction of plasma plume with biomaterial, the effect of additive O₂ gas on the optical spectrum is also explored. Then, using a fast ICCD camera, the temporal and spatial evolutions of the plasma inside the plume are elucidated. Dependence of bullet behavior on the applied voltage and the duty cycle is investigated. As an example of plasma-living tissue interaction, the application of the plasma jet in the treatment of human breast cancer cell is presented. Apoptosis, or programmed cell death, is a genetically regulated process occurring naturally in response to a variety of signals and resulting in numerous cellular changes such as membrane blebbing, cell shrinkage, nuclear condensation, DNA fragmentation, and formation of apoptotic bodies. A preliminary experiment on the apoptotic effect of the plasma jet on human breast cancer cell is performed.

II. EXPERIMENTAL

Our plasma jet device consists of a quartz confinement tube, two electrodes, Teflon fitting, and a funnel-shaped nozzle. This device is designed with some modifications to the discharge concept introduced by Zhang *et al.*^{2,13} A schematic diagram is shown in Fig. 1. A quartz tube (6 mm i.d. × 8 mm o.d., 20 mm L) served as the dielectric barrier layer. At the center of the quartz tube, a stainless steel capillary tube (0.4 mm i.d. × 1 mm o.d., fixed by a perforated Teflon fitting) was used as the power electrode as well as the O₂ feeding tube. The small outside diameter of the capillary electrode with a sharp edge allows for the local enhancement of the electric field and thus, a considerable reduction of the breakdown voltage requirement. Compared to the similar source,^{2,13} the plasma discharge can be sustained at much reduced voltage in this device. A funnel-shaped quartz nozzle (2 mm i.d. × 4 mm o.d.) was attached to the end of the quartz tube. The distance between the end of the steel tube and the end of quartz tube was approximately 2 mm. The Al foil strip of 11 mm in length

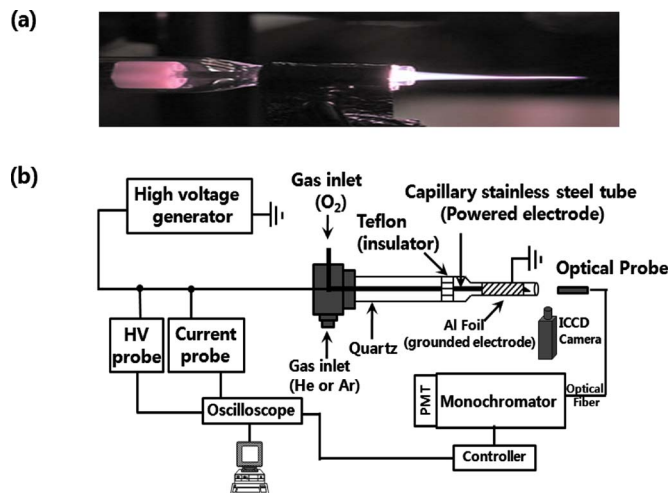


FIG. 1. (Color online) (a) Photograph of the jet/plume from the quartz tube and (b) schematic of the experimental setup with diagnostics systems.

was used as the ground electrode covering partially the outside of the quartz tube. The plasma-forming gas (He or Ar) was fed through the side of the tube, while the reactive gas O₂ was injected through the power electrode and mixed with the He or Ar plasma at the end of the quartz tube. Three different power supplies are employed. The pulsed power supply (PDS4000, FTLab) delivers microsecond (or several hundreds of nanosecond) voltage pulses of up to 3 kV at repetition rates from 10 to 60 kHz. The sinusoidal voltage source of several tens of kilohertz (HPSI200 FTLab) is applied to the tungsten wire. The RF power source (YS E03F) of 13.56 MHz can also be applied to the wire through a matching network.

The waveforms of the voltage and the current were measured using a real time digital oscilloscope (LeCroy WS44XS-A) via high voltage probe (Tektronix P5100) and current probe (Pearson 3972). To identify reactive species that are generated in the discharge and subsequently expelled with the gas flow, optical spectra were recorded for emission along the axis of the jet in the range from 200 to 900 nm. The light emitted by the microplasma was focused by means of optical fiber into entrance slit of 0.75 m monochromator (SPEX 1702), equipped with a grating of 1200 grooves per millimeter and slit width of 100 μm . A fast ICCD camera (Princeton Instruments, Model PIMAX2) was used to capture the dynamics of the discharge.

The interaction of the plasma jet with a living tissue was examined on human breast cancer cells. Human breast cancer cell line (MCF-7) was propagated in Dulbecco's modified Eagle's with 10% fetal bovine serum and 100U/ml penicillin. Cells were incubated at 37 °C with humidified air and 5% CO₂. Then cells were plated in Lab-Tek chamber slides (Nunc™) at a density of 0.5×10^6 cells per chamber, incubated overnight, and exposed to the Ar plasma plume for 20 s. Prior to plasma treatment, media from each chamber were almost removed and a small amount (200 μl) of media was left to keep cells wet during treatment. The distance from the nozzle to the cell surface was 10 mm. The plasma plume directly reached the cell. Apoptosis can be detected in

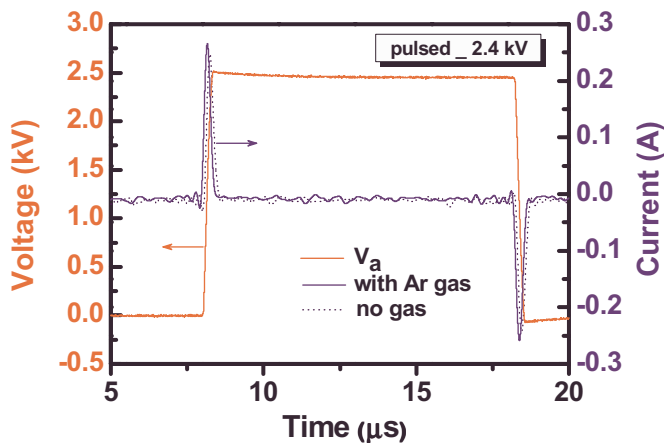


FIG. 2. (Color online) Waveforms of voltage and total current.

many ways: by visual observation of the cell shape, by staining of the cell's DNA with propidium iodide followed by microscopic detection of condensed DNA pieces, by staining externalized phosphatidyl serine (Annexin V assay), etc.¹⁴ In this work, after treatment, the culture was allowed to propagate by adding 1 ml of fresh media. Since cell growth slows down significantly, the number of dead cells increases 24 h after treatment.¹⁵ At 48 h after treatment, DAPI (4', 6-diamidino-2-phenylindole) was dropped to the fixed cells and changes in nuclear morphology were detected by fluorescence microscopy (Micros, MCX 500).

III. RESULTS AND DISCUSSIONS

When a pulsed dc voltage of amplitudes up to 3 kV, repetition rates up to 60 kHz, and duty cycles variable from 5% to 95% is applied to the power electrode and helium or argon gas is injected into the quartz tube with flow rates from 1 to 8 l/min, the homogeneous plasma is generated and is launched through the end of the tube into the surrounding air. Under typical operating conditions, a glow discharge fills the entire annular space contained between the quartz tube and the capillary electrode. By varying the pulse width (via duty cycle) and the pulse period (via repetition rate) it is possible to modify and, in fact, determine the plasma mode; for example, it is possible to force filaments to be created, allowing their formation to be investigated, or to prevent them from appearing and staying in the glow mode.¹⁶

Figure 2 shows the wave forms of the applied voltage and total current for the pulsed discharge operating at a repetition rate of 50 kHz. The gas flow rate was kept constant at 2 l/min. To find out the actual discharge current, the displacement current (I_{no}) is subtracted from the total current (I_{tot}). For the applied voltage amplitude 2.5 kV, the peak total current is 0.26 A. The discharge current is about 20 mA. The plasma plume has a cylindrical shape. The length of the plasma plume can be adjusted by the gas flow rate and the applied voltage. The plume length, which is indicative of the distance many reactive species can extend into the ambient atmosphere, is shown as a function of applied voltage for He and Ar jets at the gas flow rate of 1 l/min in Fig. 3. The plume length increases with applied voltage. Since it is

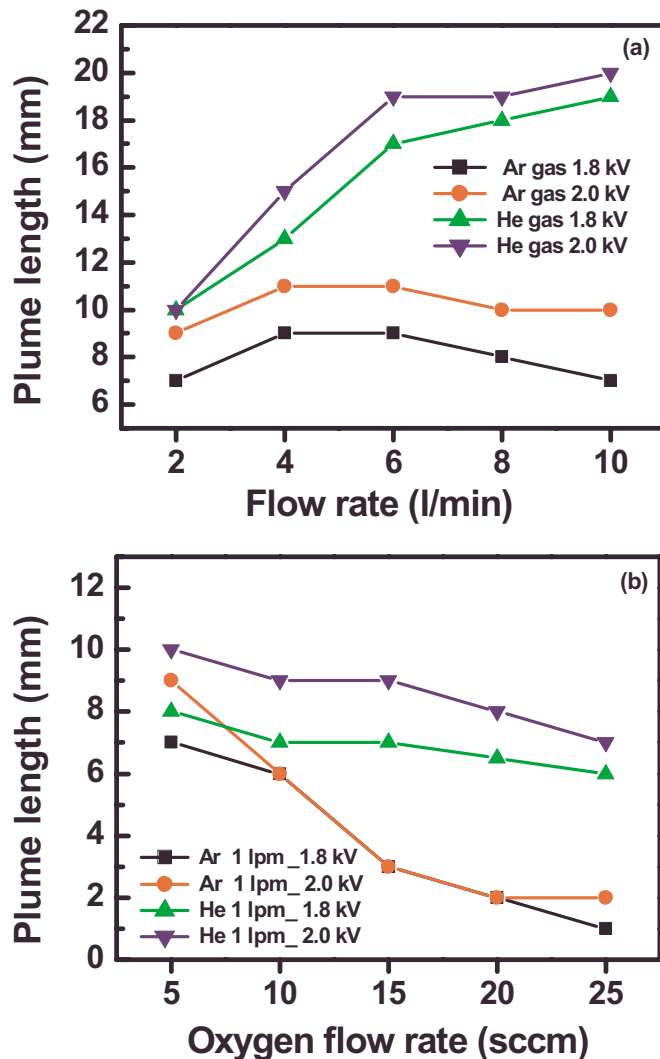


FIG. 3. (Color online) Plume length as functions of (a) gas flow rate of He and Ar gas (b) of the additive oxygen flow rate for the He and Ar jet (at the applied voltage 1.8 and 2.0 kV).

mainly the electrons that play an important role in the plasma generation, the electron oscillatory displacement is related to the plasma length.¹⁷ The plasma plume length versus the gas flow rate was measured. Generally, the plasma plume length increases with the gas flow rate. Usually the increasing of the helium feeding results in jet elongation, while further increase (here, up to 8 l/min) in the flow rate caused jet shortening and appearance of a turbulent tail at the jet's end. However, in the Ar jet, the plume length first increases with gas flow rate and has a maximum and then decreases slightly or saturates.

To produce more radicals in the gas phase, O_2 was injected into the capillary tube while Ar and He were fed through the quartz tube. Adding O_2 directly into the feeding gas tends to diminish the production of radicals due to the electron attachment to oxygen inside the nozzle.¹⁸ The plume length decreases as the O_2 flow rate increases. When O_2 was injected into the He plasma at a rate of 10 SCCM (SCCM denotes cubic centimeter per minute at STP), it did not disturb the voltage-current characteristics, but a small but noticeable change in the plume length was observed. However,

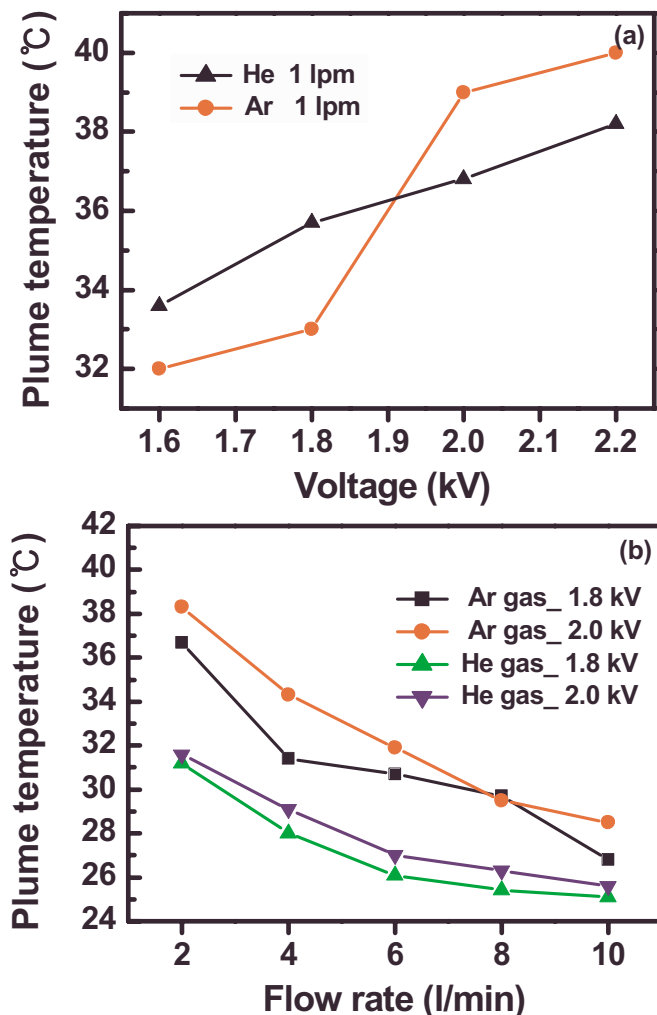


FIG. 4. (Color online) Measured plume temperature as a function of (a) applied voltage (at 1 l/min) and of (b) gas flow rate (at 1.8 and 2.0 kV) for the He and the Ar jet.

the plume length began to decrease above 15 SCCM and the plume color whitened when the O_2 flow rate was higher than 20 SCCM. In the Ar plasma jet, the plume length began to decrease rapidly with the O_2 flow rate. Oxygen concentration ratio exceeding 1 vol % influences the plasma discharge so severely that maintaining the plasma column needs raising the applied voltage to a higher value. The plume length is also correlated with the distance that reactive species travel into the ambient.

Figure 4 shows the measured plume temperature as functions of the applied voltage and the flow rate. The plume temperature was measured by using a fiber optic temperature sensor (Luxtron M601-DM&STF). The continuous increase in the plume temperature can be seen as the applied voltage increases. An increase in the applied voltage leads to the increase in the plasma volume, which is immediately reflected by gas heating. The plume temperature decreases as the gas flow rate increases. The plume temperature (T_g) of the plasma can be also deduced from the rotational temperature (T_r) of diatomic species, which is expected to be in equilibrium with T_g . The rotational temperature of a molecule can be obtained by comparing the synthetic diatomic

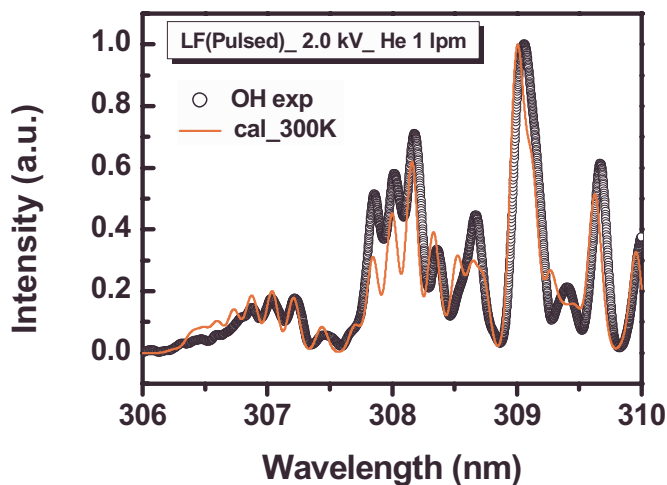


FIG. 5. (Color online) Comparison of experimental and simulated spectra of OH ($A^2\Sigma^+ \rightarrow X^2\Pi$, 306–310 nm) transition for T_r measurement of the He jet (2.0 kV, 1 l/min).

molecular spectrum with measured one.¹⁹ To obtain the best fit between the experimental and the synthetic spectral bands, a least-square procedure is used. A typical fitting of the measured band spectrum with the synthetic spectrum is shown in Fig. 5. The fine structure of the rotational band of OH ($A^2\Sigma^+ \rightarrow X^2\Pi$ transition) from 306 and 310 nm is fitted to obtain the gas temperature. The simulated spectrum at $T_r = 300$ K gives the best fit to the experimental spectrum.

Another method to determine the plume temperature is to utilize the line shape of the transition. As is well known, the line profile of an emission line results from the contribution of different mechanisms: the Doppler broadening $\Delta\lambda_{Dopp}$ and the instrumental broadening $\Delta\lambda_{inst}$ cause the appearance of Gaussian profiles ($\Delta\lambda_G = \Delta\lambda_{inst} + \Delta\lambda_{Dopp}$), while the natural broadening $\Delta\lambda_{nat}$, resonance broadening $\Delta\lambda_{res}$, van der Waals broadening $\Delta\lambda_{vdW}$, and Stark broadening $\Delta\lambda_{Stark}$ can be approximated by Lorentzian profiles ($\Delta\lambda_L = \Delta\lambda_{nat} + \Delta\lambda_{vdW} + \Delta\lambda_{Stark} + \Delta\lambda_{res}$). The shape and the full width at half maximum (FWHM) of the instrumental broadening $\Delta\lambda_{inst}$ are deduced by recording the Ne line emitted by a He–Ne laser. A typical line is presented in Fig. 6(a). The best fit is the Gaussian function, and its FWHM is given in the figure. From the resulting Lorentzian contribution, the Stark broadening is obtained after subtracting the van der Waals contribution. From this, electron density values can be obtained for Ar and He plasmas. In our experimental conditions, however, the Stark broadening is too small since the electron density of the plasma jet is on the order of 10^{-12} cm⁻³, also $\Delta\lambda_{nat}$ and $\Delta\lambda_{res}$ are negligible compared to the other effects.²⁰ The effect of Doppler broadening has been determined using the expression, $\Delta\lambda_{Dopp} = 7.16 \times 10^{-7} \lambda (T_g/M)^{1/2}$ (λ is the wavelength in angstrom, T_g is the temperature of the emitter in kelvin, and M is the atomic weight in g mol⁻¹). Therefore, the main contribution to the broadened profiles is due to collisions (van der Waals broadening) and the apparatus function (instrumental broadening). The line shape of the transition is determined by Lorentzian (Stark, van der Waals, resonance, natural) and Gaussian (Doppler, instrumental) broadening mechanisms that result in

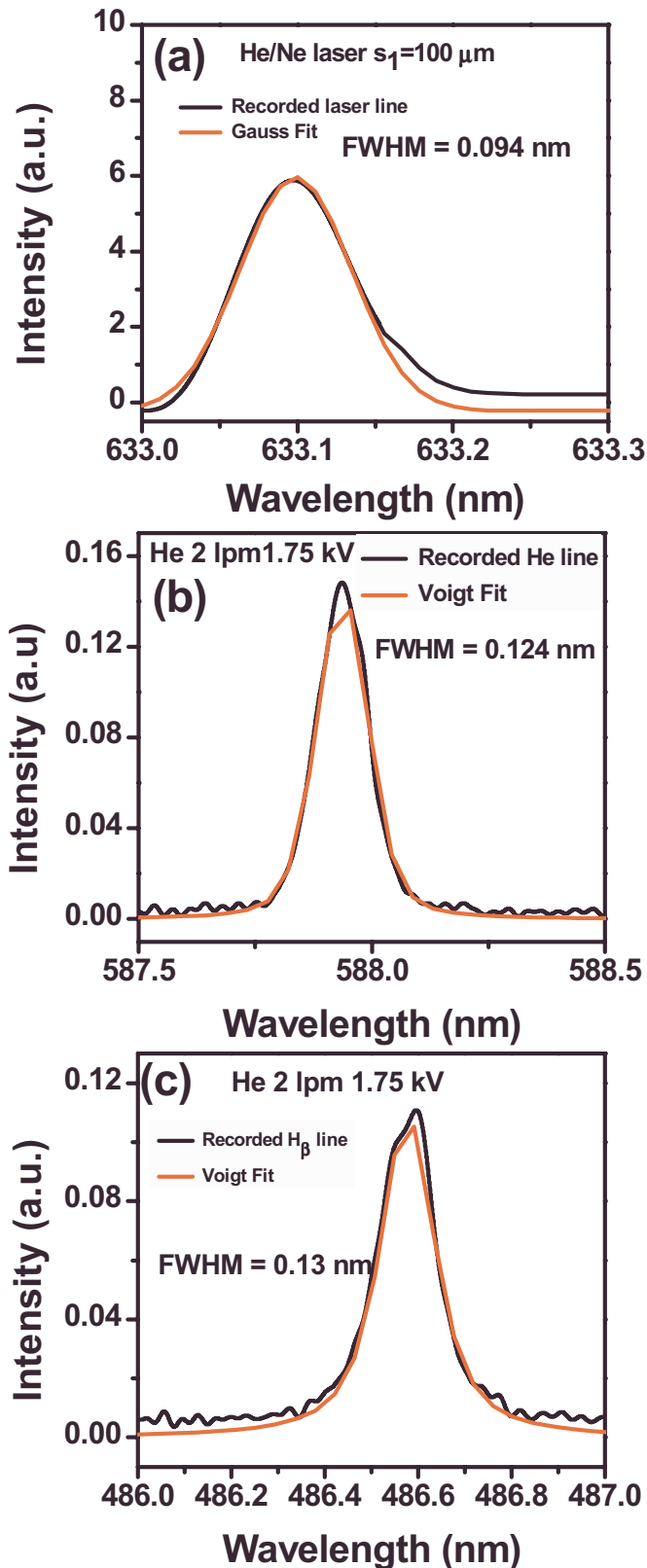


FIG. 6. (Color online) (a) Recorded line and Gaussian fit of the He–Ne laser radiation, (b) recorded He line and Voigt fit, and (c) H_{β} line shape obtained from the experiment and Voigt fit.

a Voigt profile. The $\Delta\lambda_v$ is the FWHM of the Voigt shape line, and it is related to $\Delta\lambda_L$ and $\Delta\lambda_G$ through the relation $\Delta\lambda_G^2 = \Delta\lambda_v^2 - \Delta\lambda_v\Delta\lambda_G$.²¹ An analysis of spectral line profiles is used to calculate the gas temperature in an atmospheric

pressure plasma jet. Two transitions are studied, that of He at 587.5 nm and that of hydrogen (H_{β}) at 486.1 nm.²¹ For the He 587.5 nm, one obtains

$$\Delta\lambda_v^2 - (\Delta\lambda_v)(25.6 \times T_g^{-7/10}) - (\Delta\lambda_{\text{inst}} + 2.1 \times 10^{-3}\sqrt{T_g})^2 = 0. \quad (1)$$

The same procedure is applied to the H_{β} line, and the general expression to be used for deducing the gas temperature is

$$\Delta\lambda_v^2 - (\Delta\lambda_v)(29.12 \times T_g^{-7/10}) - (\Delta\lambda_{\text{inst}} + 3.48 \times 10^{-3}\sqrt{T_g})^2 = 0. \quad (2)$$

Since the values $\Delta\lambda_{\text{inst}}=0.94$ Å, $\Delta\lambda_v=1.24$ Å (He), 1.3 Å (H_{β}) are measured as shown in Figs. 6(a)–6(c), the calculated plume temperatures using Eqs. (1) and (2) are 301 K (He) and 306 K (H_{β}). These temperatures are well in agreement with ones obtained from the intensity distribution of OH rotational lines and by the optical fiber thermometer. Therefore, the plume temperature is practically room temperature. This plasma jet can be employed for biomedical applications. However, in the RF excitation, the plume temperature rises up to 330 K.

Figure 7 shows the emission spectra observed in the He plasma for three different power supplies (pulsed wave with a repetition rate of 50 kHz, 50 kHz sinusoidal wave, and 13.56 MHz RF wave). It shows that there are strong nitrogen molecular lines as well as a few helium and oxygen atomic lines. The strongest emission is the N_2^* line at 337.2 nm ($C^3\Pi_u \rightarrow B^3\Pi_g$), and many nitrogen lines, excited He atom line at 706.5 nm, and excited oxygen line at 777 nm are shown. Oxygen and nitrogen species arise because the plasma is ejected into the ambient air where its energetic electrons and He metastables ionize and excite air molecules. The N_2^+ line at 391 nm ($B^2\Sigma_u^+ \rightarrow X^2\Sigma_g^+$) is attributed to Penning ionization ($He^* + N_2 \rightarrow He + N_2^+ + e^-$) and charge transfer ($He^+ + N_2 \rightarrow He + N_2^+$) (Ref. 22) followed by direct electron-impact excitation ($e^- + N_2^+ \rightarrow N_2^{*+} + e^-$). The excited He is capable of exciting and ionizing a considerable amount of nitrogen molecules taking into account air molecule composition. Stronger excited N_2^+ emission was observed for the pulsed plasma jet than the sinusoidal wave driven plasma jet. Atomic oxygen is generally generated by a dissociative collision between an oxygen molecule and an electron. Atomic oxygen may also be generated through Penning ionization ($N_2^* + O_2 \rightarrow N_2 + O + O$). Active species generated in the microplasma jet carry enough energy to remain active in spite of their transference to the free environment. The emission spectrum clearly indicates that OH (309 nm) and NO (283 nm) exist in the plasma plume.² The emission line at 656 nm corresponds to the H_{α} line, which is generated by the collision between water vapor molecule and electrons ($H_2O + e \rightarrow H + OH + e$). The emission intensity of OH at 309 nm is stronger than that of H_{α} at 656 nm. This indicates that OH radicals are also formed by the reaction of excited O with water vapor molecule ($H_2O + O \rightarrow 2OH$), in which O (1D) is a product of the reaction $e + O_2 \rightarrow O(^3P) + O(^1D) + e$, which requires electrons of at least 3.1 eV.² Daily variations in the laboratory atmospheric humidity levels could affect

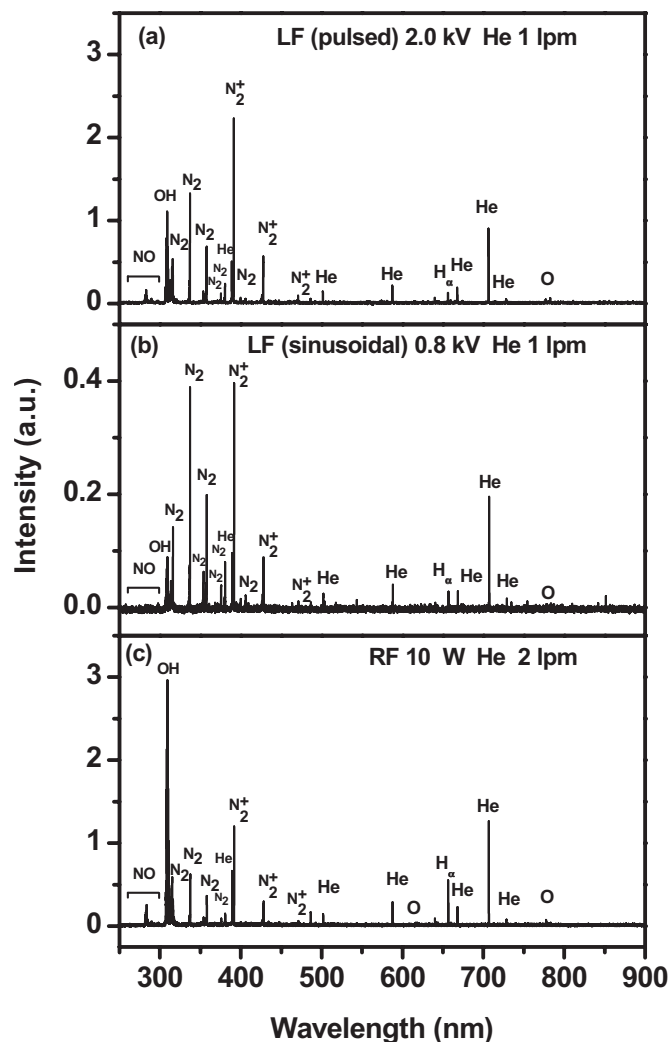


FIG. 7. Emission spectra from 200 to 900 nm observed in the He jet driven by (a) pulsed wave (2.0 kV, 1 l/min), (b) sinusoidal wave (0.8 V_{rms}, 1 l/min), and (c) RF power (10 W, 2 l/min).

the measured OH number densities. The OH emission is enhanced in the RF plasma. This is caused by higher electron density and electron temperature in the RF plasma. The NO serves a multitude of essential biological functions including the bactericidal effect and the induction of the phagocytosis of bacteria and necrotic detrite. These highly reactive species (O, OH, and NO) are considered to be most effective agents in attacking cells or organic material in general. In addition to these, high concentration of ozone is measured as a result of various secondary reactions in RF discharge. It should be noted that the peak intensity is not directly proportional to the excited state density of the species. The relative spectral response of the detection system employed in this work is as follows: 0.420 (283 nm), 0.502 (309 nm), 0.479 (337 nm), 0.448 (391 nm), 0.0368 (706 nm), and 0.0108 (777 nm). Although the intensities of peaks with wavelength above 600 nm seem small, the concentrations of the excited states of those species are not small actually. The pulsed discharge maintains almost the same level of the emission intensity to those of the RF discharge. This indicates that a low-frequency pulsed operation of the plasma jet can provide

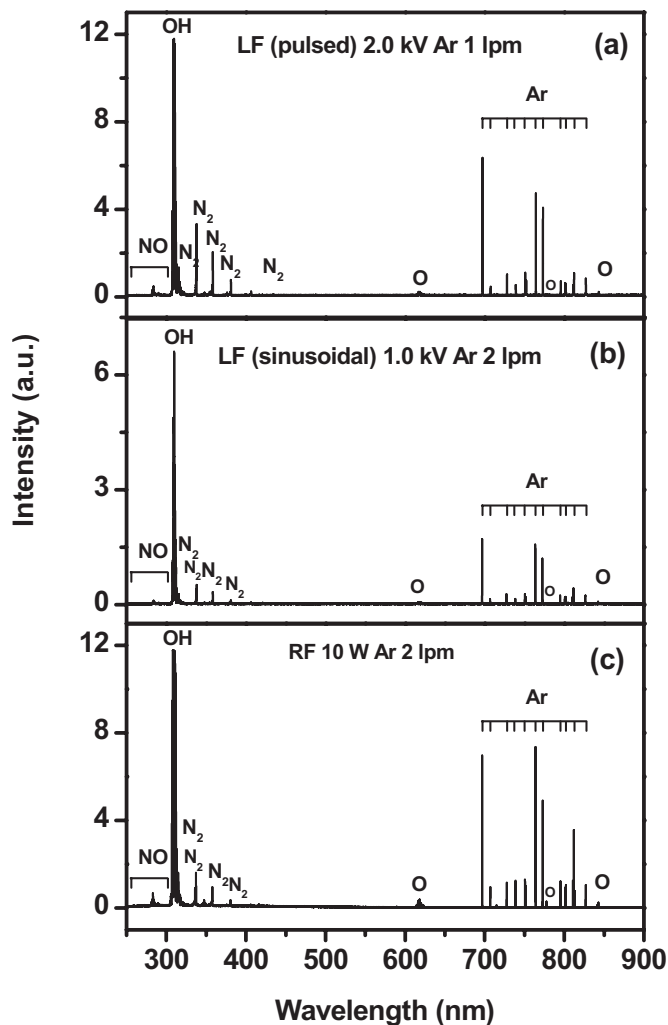


FIG. 8. Emission spectra from 200 to 900 nm observed in the Ar jet driven by (a) pulsed wave (2.0 kV, 1 l/min), (b) sinusoidal wave (1.0 V_{rms}, 2 l/min), and (c) RF power (10 W, 2 l/min).

sufficient amount of radicals without the gas temperature rise. To produce more radicals in the gas phase, we added O₂ into downstream of He plasma through the capillary steel tube. The addition of oxygen to the He plasma decreases the emission intensities from He and nitrogen molecules, except for the He line (667 nm). This suggests that some electrons were probably consumed to produce O radicals when O₂ was injected into the He plasma zone.^{2,13}

Figure 8 shows the emission spectrum observed in the Ar plasma driven by (a) pulsed wave (2.0 kV, 1 l/min), (b) sinusoidal wave (1.0 V_{rms}, 2 l/min), and (c) RF power (10 W, 2 l/min). There appeared many Ar peaks corresponding to 4p → 4s transitions. The atomic oxygen lines of 616 and 777 nm, excited N₂ lines at 337 nm and at 357 nm can be found in the emission spectrum. It has been known that the atmospheric pressure Ar/O₂ plasma is relatively difficult to sustain in comparison with He/O₂ plasma and it produces more reactive oxygen radicals and metastable oxygen species such as O*(¹D), O₂*(¹Δ_g), as the electron density of Ar plasma is nearly twice that of He plasma at atmospheric pressure.^{23,24} However, a little different spectrum was obtained in this work. Even with additive oxygen flow, the

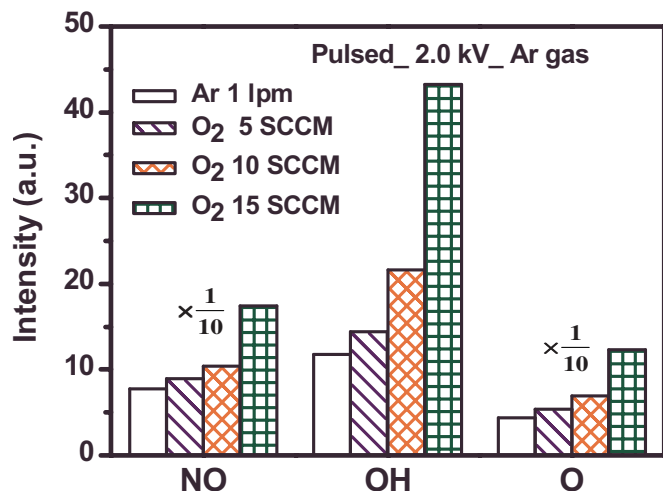


FIG. 9. (Color online) Variations of the emission intensities from NO, OH, and O as a function of the amount of additive O₂ for the pulsed Ar jet.

oxygen peaks were weak in contrast to much stronger OH peak. Since the OH emission originates from the fragmentation of water molecules that desorbs from the quartz tube, the drastic increase in OH peak when the discharge is operated in Ar is probably a consequence of the increase in the electron density and electron energy. The effect of the additive oxygen flow was insignificant. As can be seen in Fig. 8, the emission intensity of the Ar/O₂ plasma jet plume is significantly higher than that of the He/O₂ plasma plume over the entire spectral range. Compared to the earlier works,² the Penning ionization of N₂ and the charge transfer to N₂⁺ are relatively suppressed in the Ar discharge. Therefore, the peaks associated with nitrogen molecules are relatively diminished due to the lack of exciting agent such as He metastables.

Figure 9 shows the variations of NO, OH, and O with the amount of O₂ addition for the Ar pulsed jet. The additive O₂ gas increases the emission intensities from NO, OH, and O. The variations of NO, OH, and O with the O₂ addition show slightly different behaviors, which are dependent on the plasma properties such as electron energy distribution function, electron density, electron temperature, and the concentrations of various species. These are related to the experimental parameters and to the type of power supply. The concentration of atomic oxygen in the plasma discharge is critical for improving the operating efficiency and treatment effect. Earlier study also showed that OH and O radicals increase with the addition of O₂.² Although not shown in figure, for the He jets, the strongest oxygen emissions were observed with an oxygen flow rate of 5 SCCM. In some cases, the NO lines can decrease with the additive O₂. Several reasons can cause the observed decrease at higher O₂ admixtures. One could be the altered discharge characteristics, for example the electron energy distribution function. Moreover, further oxidation of NO may play a role at higher air admixtures, for example reactions with molecular oxygen to produce NO₂.²⁵ The intensities of NO, OH, and O were proportional to the RF power. For RF powers beyond 30 W the discharge eventually switches into another more inhomogeneous

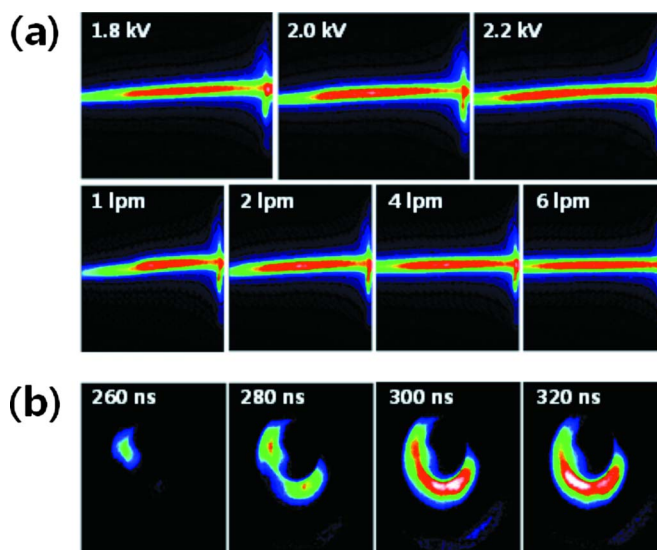


FIG. 10. (Color online) (a) Side view (1.8–2.2 kV, 1–6 l/min) of the accumulated ICCD image of the pulsed Ar jet under the shutter mode. (b) Front view of the jet under the gate mode (1.8 kV, 2 l/min).

geneous γ -discharge mode which has to be avoided.

Images of the discharge were captured using an ICCD camera, and the propagation velocity of the plasma bullet was also determined. Figure 10(a) shows the side view of ICCD images of the pulsed Ar plasma jet under the shutter mode. The shutter mode integrates time for 10 ms with a gain of 1.0. The side view indicates that the plume length depends mainly on two parameters: the applied voltage and the gas flow rate. The plume length and intensity increase with the applied voltage and the gas flow rate. Figure 10(b) shows the front view (sequent ones) of the jet under the gate mode. The front view reveals that the bullet has a hollow donut-shaped structure.

In Fig. 11, a series of photographs of the pulsed Ar plasma plume starting from the time the plume can be captured with an exposure time of 20 ns, taken by use of an ICCD camera, are presented. Every single shot was synchronized with the supply voltage. The sequent images are taken with the gate mode at every 20 ns. The number of accumulation time is 3000 for the gate mode.²⁶ High-speed photographs taken in the voltage rising phase for various conditions (applied voltage and duty cycle) are compared in (a)–(d). It can be seen that the jet is not constant in time but rather a moving plasma bullet coming out of the tube with a velocity that is much higher than the gas flow velocity. For the pulsed voltage of 2.0 kV, the bullet covers a distance of around 3.9 mm in 180 ns. This corresponds to an average velocity of 2.2×10^4 m/s. The bullet always appears in the rising slope of supplying voltage.

In each pulse of the discharge current, one plasma bullet is produced. During a sufficiently long period of time the atmospheric pressure plasma jet is essentially a fast-moving train of plasma bullets with 10 μ s between two sequential plasma bullets for the duty cycle of 50%. As a plasma bullet traveled from the outlet of the quartz tube, its optical signature changed its intensity and size. When the discharge current starts to go up, it marks the emergence of a plasma

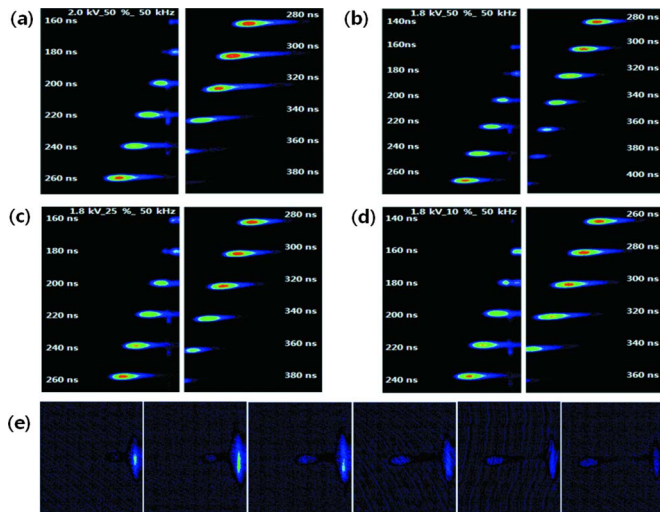


FIG. 11. (Color online) High-speed photographs of the pulsed Ar plasma plume taken under the gate mode in the voltage rising phase for various conditions (applied voltage and duty cycle); (a) 2.0 kV, 50%, (b) 1.8 kV, 50%, (c) 1.8 kV, 25%, and (d) 1.8 kV, 10%. The pulse repetition rate is 50 kHz and the flow rate is 2 l/min. (e) Image of plume in the voltage falling phase. The duty cycle is 50%.

bullet from the dielectric tube. The discharge current reached its peak value at a time delay of 280 ns, and the intensity of the plasma bullet also became strongest. It resembles a cathode-oriented streamerlike discharge. This suggests that during the rising phase of the discharge current, the plasma bullet grew and became stronger, as shown in Fig. 11. The velocity of the plasma bullets increased in this period. After that, the plasma bullet started to die off as the discharge current started to decline. During this current-falling phase, there were fewer sufficient energetic electrons to produce relevant excited plasma species resulting in a diminishing optical emission. As can be seen from the high-speed photographs, the streamer head is connected to the power electrode by highly conducting channel. A weak plasma bullet was observed during the voltage-falling phase. This corresponds to a new breakdown of the gap. This discharge ignites because of the voltage induced by the charges, which have accumulated on the surface of the dielectric tube during the previous discharge. As can be seen from the figure, the plasma bullet velocity increases with the applied voltage and it decreases with the duty cycle. Figure 11(e) shows that the image in the voltage falling phase is much weaker and the bullet is traveling at a slower speed, compared to the image of plasma bullet in the rising phase of the applied voltage.

Since at atmospheric pressure the recombination rate is so high, any real transport of reactive species from the plasma source over several centimeters will not work quantitatively. It is more likely that the excitation is due to an ionization wave along the gas channel and is triggered by the kilohertz excitation inside the source. This excitation might cause local dissociation of the source gas along that gas channel. Therefore, it is possible to state that the plasma bullet is produced by the ionization wave front. There are three mechanisms to contribute to the ionization front velocity, namely, the electron diffusion, the ponderomotive force,

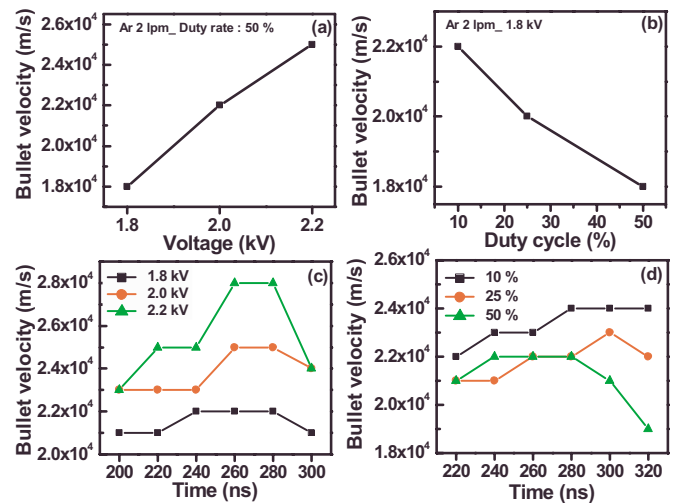


FIG. 12. (Color online) Average bullet velocity vs (a) the applied voltage and (b) the duty cycle. Bullet velocities for several values of (c) the applied voltage and (d) the duty cycle vs time.

and the breakdown wave.^{10,11} The ionization wave front velocity due to electron diffusion can be expressed as $v = 2(v_i D_a)^{1/2}$, where v_i is the ionization frequency and D_a is the ambipolar diffusion coefficient. For a nonequilibrium plasma, D_a is expressed as $D_a = \mu_+ k_B T_e / e$, where μ_+ is the ion mobility and k_B is the Boltzmann constant. In the case of Ar ions, $\mu_+ = 1.315 \text{ cm}^2 \text{ V}^{-1} \text{ s}^{-1}$. The frequency of Ar ionization by electrons is estimated to be about $3.6 \times 10^{11} / \text{s}$ and the electron temperature is estimated to be 0.4 eV from the modified Boltzmann plot method utilizing the Ar 4p \rightarrow 4s transitions in the optical spectrum.²⁷ With these parameters, the velocity of the ionization wave front is calculated as $8.7 \times 10^3 \text{ m/s}$. This is close to the bullet velocity. Given that only the electron diffusion mechanism is considered and our estimate of the electron temperature is based on the corona balance which is too simplistic at atmospheric pressure, this agreement is particularly encouraging. The two other mechanisms of the ionization wave, namely, the ponderomotive force and the breakdown wave, depend on the gradient of the electric field. They are likely to add to the ionization front velocity estimated from electron diffusion only and thus bring the overall speed of the ionization wave front closer to the plasma bullet velocity of $2.2 \times 10^4 \text{ m/s}$.¹¹

As was shown in Fig. 10(b), the front view of the bullet is revealed to be “donut” shaped. This gives an indication that solitary surface ionization waves may be responsible for the creation of these bullets.¹² Another interesting fact is that the total time lapse of the jet propagation is nearly independent of the pulse repetition rate. As shown in Fig. 12, the plasma bullet accelerates in the first 80 ns, and reaches a maximum velocity of $2.8 \times 10^4 \text{ m/s}$ (for the applied voltage of 2.2 kV). Note that the maximum bullet velocity is reached at approximately the same position as that where the largest bullet size (and luminosity) is reached. After that, the bullet decelerates and finally extinguishes. The gas flow velocity of Ar in the exit quartz tube is estimated to be 8.8 m/s (for the gas flow rate of 2 l/min), some four orders of magnitude lower than the bullet velocity. The propagation of the bullet

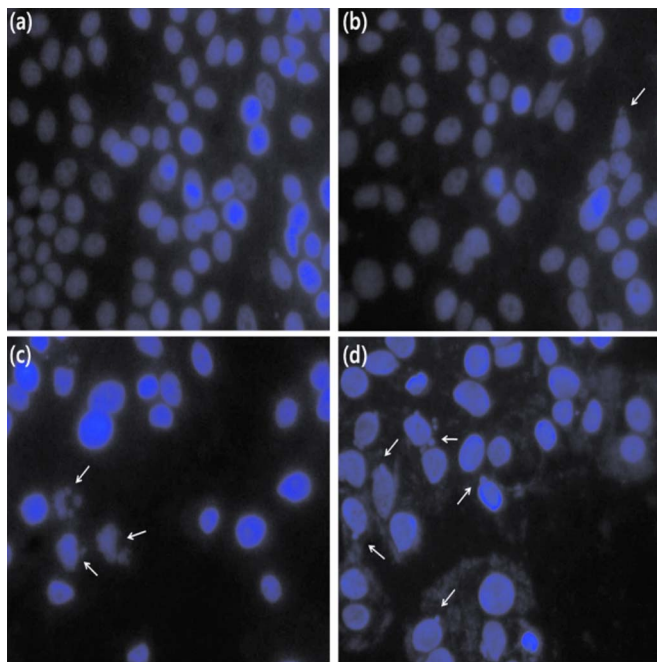


FIG. 13. (Color online) MCF-7 cells were stained with DAPI, and observed under fluorescence microscopy at a magnification of $400\times$; arrows indicate apoptotic cells. The images observed in the pulsed Ar plasma jet with different conditions: (a) nontreated control, (b) Ar only, (c) Ar with the 5 SCCM of oxygen gas, and (d) Ar with the 10 SCCM of oxygen gas.

is almost independent of the gas flow rate. However, the propagation of the bullet is not independent of the form of the applied voltage contrary to the observations of Teschke *et al.*⁴ The speed of the plasma bullets has a range from 1.9×10^4 to 2.8×10^4 m/s. The plasma bullet velocity is found to increase with the applied voltage but to decrease with the duty cycle. This can be accounted for from that an increase in the applied voltage results in a higher electron drift velocity thereby increasing the ionization wave front velocity. On the other hand, a larger duty cycles elongates the time span of the propagation of bullet, and the average velocity of bullet decreases. At low duty cycles the pulse width decreases. Then the intervals between the primary discharge (due to the positive current pulse) and the weak discharge (due to the negative current pulse) are shortened. This might cause the electric field gradient to be strong thereby increasing the bullet speed.

Figure 13 shows the fluorescence image of cells among treated and untreated populations. Cells treated for 20 s were then incubated and stained for DNA fractionation 48 h later. The images were obtained in the pulsed Ar plasma jet with different conditions: (a) nontreated control, (b) Ar only, (c) Ar with the 5 SCCM of oxygen gas, and (d) Ar with the 10 SCCM of oxygen gas. It shows that the addition of a small amount of O_2 gas to pure argon results in more significant apoptotic behavior. Apoptosis is an internally released mechanism of cellular self-destruction. The cell falls apart in several membrane-bound apoptotic bodies. The changes in nuclear morphology were detected by DAPI staining. Following the DAPI stain procedure, it was observed that a significant portion of these cells exhibits the apoptotic frag-

mentation as is evident from the figure. As was observed in Fig. 9, the active radicals were higher in the O_2 flow rate of 10 SCCM. As can be seen in Fig. 13(d), more apoptotic bodies were observed in the O_2 flow rate of 10 SCCM than those in the O_2 flow rate of 5 SCCM, indicating that the apoptosis is related to these radicals. From the comparison of (a)–(d), it can be stated that the primary role in the apoptosis was played by reactive oxygen species such as O, NO, and OH species in the plasma plume.

IV. CONCLUSION

The atmospheric pressure microplasma jet described in this study employed a quartz tube of 36 mm long, one end of which was wrapped with an Al foil strip of 11 mm as the grounded electrode. A capillary stainless steel tube was used as the power electrode and the gas exit of the additive O_2 gas. The electrode was driven by power supply at an excitation frequency either in several tens of kilohertz ac range (or pulsed voltage with repetition rates of kilohertz range) or in RF range. The jet source proved to operate stably and to provide plasma plume at near room temperature under a variety of operating conditions except the RF case. The low-frequency pulsed operation of the plasma jet can provide sufficient amount of radicals without the plume temperature rise, which makes it suitable for biomedical applications. A small amount of the additive O_2 gas increases the emission intensities from O, NO, and OH (thus concentrations of these species).

To better understand the dynamics of the plasma plume, a high-speed ICCD camera was used to capture the temporal behavior of plasma bullet. It is found that the plasma plume is not a continuous volume of plasma but rather a moving plasma bullet and that in front view the bullet is hollow and has a “donut” structure. For the applied voltage 2.0 kV pulsed wave, the average velocity of the plasma bullet was 2.2×10^4 m/s. The plasma bullet velocity increases with the applied voltage but decreases with the duty cycle. The length of the plume depends mainly on two parameters: the applied voltage and the gas flow rate. The plume length and intensity increase with the applied voltage and the gas flow rate. The plasma bullet velocity is found to increase with the applied voltage but to decrease with the duty cycle. A gas breakdown taking place in the case of a needle-shaped electrode creates a nonuniform electric field and causes the ionization wave to propagate in the form of a streamer. Therefore, the plasma bullet has both the characteristics of a cathode-oriented streamer and of the ionization wave. It was observed that a significant portion of human breast cancer cells exhibit apoptotic fragmentation with the application of the plasma jet and a small amount of the additive O_2 gas promotes the apoptosis.

ACKNOWLEDGMENTS

Helpful discussions with Mr. Chang-Seung Ha, Professor Ho-Jun Lee, and Professor Hae June Lee of Pusan National University are greatly acknowledged. This work was supported by the National Research Foundation of Korea under Contract No. 2009-0067223.

- ¹M. Laroussi and T. Akan, *Plasma Processes Polym.* **4**, 777 (2007).
- ²X. Zhang, M. Li, R. Zhou, K. Feng, and S. Yang, *Appl. Phys. Lett.* **93**, 021502 (2008).
- ³T. L. Ni, F. Ding, X. D. Zhu, X. H. Wen, and H. Y. Zhou, *Appl. Phys. Lett.* **92**, 241503 (2008).
- ⁴M. Teschke, J. Kedzierski, E. G. Finantu-Dinu, D. Korzec, and J. Engemann, *IEEE Trans. Plasma Sci.* **33**, 310 (2005).
- ⁵A. Fridman, A. Chirokov, and A. Gutsol, *J. Phys. D: Appl. Phys.* **38**, R1 (2005).
- ⁶X. T. Deng and M. G. Kong, *IEEE Trans. Plasma Sci.* **32**, 1709 (2004).
- ⁷N. Jiang, A. Ji, and Z. Cao, *J. Appl. Phys.* **106**, 013308 (2009).
- ⁸S. Wang, V. Schulz-von der Gathen, and H. F. Döbele, *Appl. Phys. Lett.* **83**, 3272 (2003).
- ⁹X. Lu and M. Laroussi, *J. Appl. Phys.* **100**, 063302 (2006).
- ¹⁰X. Lu, Q. Xiong, Z. Xiong, J. Hu, F. Zhou, W. Gong, Y. Xian, C. Zou, Z. Tang, Z. Jiang, and Y. Pan, *J. Appl. Phys.* **105**, 043304 (2009).
- ¹¹J. Shi, F. Zhong, J. Zhang, D. W. Liu, and M. G. Kong, *Phys. Plasmas* **15**, 013504 (2008).
- ¹²N. Mericam-Bourdet, M. Laroussi, A. Begum, and K. Karakas, *J. Phys. D* **42**, 055207 (2009).
- ¹³X. Zhang, J. Huang, X. Liu, L. Peng, L. Guo, G. Lv, W. Chen, K. Feng, and S. Yang, *J. Appl. Phys.* **105**, 063302 (2009).
- ¹⁴E. Stoffels, I. E. Kieft, R. E. J. Sladek, L. J. M. van den Bedem, E. P. van der Laan, and M. Steinbuch, *Plasma Sources Sci. Technol.* **15**, S169 (2006).
- ¹⁵G. Fridman, A. Shereshevsky, M. M. Jost, A. D. Brooks, A. Fridman, A. Gutsol, V. Vasilets, and G. Friedman, *Plasma Chem. Plasma Process.* **27**, 163 (2007).
- ¹⁶N. Balcon, A. Aanesland, and R. Boswell, *Plasma Sources Sci. Technol.* **16**, 217 (2007).
- ¹⁷D. B. Kim, J. K. Rhee, B. Gweon, S. Y. Moon, and W. Choe, *Appl. Phys. Lett.* **91**, 151502 (2007).
- ¹⁸V. Leveille and S. Coulombe, *Plasma Sources Sci. Technol.* **14**, 467 (2005).
- ¹⁹S. Y. Moon and W. Choe, *Spectrochim. Acta, Part B* **58**, 249 (2003).
- ²⁰C. O. Laux, T. G. Spence, C. H. Kruger, and R. N. Zare, *Plasma Sources Sci. Technol.* **12**, 125 (2003).
- ²¹A. Ionascut-Nedelcescu, C. Carlone, U. Kogelschatz, D. V. Gravelle, and M. I. Boulos, *J. Appl. Phys.* **103**, 063305 (2008).
- ²²N. K. Bibinov, A. A. Fateev, and K. Wiesemann, *J. Phys. D: Appl. Phys.* **34**, 1819 (2001).
- ²³M. Moravej, X. Yang, G. R. Nowling, J. P. Chang, R. F. Hicks, and S. E. Babayan, *J. Appl. Phys.* **96**, 7011 (2004).
- ²⁴S.-Z. Li, J. P. Lim, J. G. Kang, and H. S. Uhm, *Phys. Plasmas* **13**, 093503 (2006).
- ²⁵A. V. Pipa, T. Bindemann, R. Foest, E. Kindel, J. Röpcke, and K.-D. Weltmann, *J. Phys. D: Appl. Phys.* **41**, 194011 (2008).
- ²⁶C.-S. Ha, J.-Y. Choi, H.-J. Lee, D.-H. Kim, and H. J. Lee, *IEEE Trans. Plasma Sci.* **36**, 970 (2008).
- ²⁷F. J. Gordillo-Vazquez, M. Camero, and C. Gomez-Aleixandre, *Plasma Sources Sci. Technol.* **15**, 42 (2006).